



HAL
open science

Pivotal role of PIM2 kinase in plasmablast generation and plasma cell survival, opening new treatment options in myeloma

Marion Haas, Gersende Caron, Fabrice Chatonnet, Stephane Manenti, Elina Alaterre, Julie Devin, Céline Delaloy, Giulia Bertolin, Roselyne Viel, Amandine Pignarre, et al.

► **To cite this version:**

Marion Haas, Gersende Caron, Fabrice Chatonnet, Stephane Manenti, Elina Alaterre, et al.. Pivotal role of PIM2 kinase in plasmablast generation and plasma cell survival, opening new treatment options in myeloma. *Blood*, 2022, 139 (15), pp.2316-2337. 10.1182/blood.2021014011 . hal-03578490

HAL Id: hal-03578490

<https://hal.science/hal-03578490>

Submitted on 1 Apr 2022

HAL is a multi-disciplinary open access archive for the deposit and dissemination of scientific research documents, whether they are published or not. The documents may come from teaching and research institutions in France or abroad, or from public or private research centers.

L'archive ouverte pluridisciplinaire **HAL**, est destinée au dépôt et à la diffusion de documents scientifiques de niveau recherche, publiés ou non, émanant des établissements d'enseignement et de recherche français ou étrangers, des laboratoires publics ou privés.



Distributed under a Creative Commons Attribution - NonCommercial 4.0 International License

Pivotal role of PIM2 kinase in plasmablast generation and plasma cell survival, opening new treatment options in myeloma

Tracking no: BLD-2021-014011R2

Marion Haas (INSERM_U1236, university Rennes 1, EFS Bretagne and university hospital, France) Gersende Caron (INSERM U917, France) Fabrice Chatonnet (Centre Hospitalier Universitaire de Rennes, France) stephane manenti (INSERM U1037, France) Elina Alaterre (Institute of Human Genetics, France) Julie Devin (Université de Toulouse, France) Céline Delaloy (INSERM_U1236, university Rennes 1, France) Giulia Bertolin (Université de Rennes, CNRS, Institut de Génétique et Développement de Rennes (IGDR), UMR 6290, France) Roselyne Viel (Université Rennes 1, H2P2, France) Amandine Pignarre (INSERM_U1236, university Rennes 1, EFS Bretagne and university hospital, France) Francisco Llamas Gutierrez (university hospital of Rennes, France) Anne Marchalot (Université de Limoges, UMR CNRS 7276, INSERM U1262, France) Olivier Decaux (CHU de Rennes, France) Karin Tarte (Faculté de Médecine, France) Laurent Delpy (CNRS, France) Jerome Moreaux (Institute of Human Genetics, France) Thierry Fest (INSERM_U1236, university Rennes 1, EFS Bretagne and university hospital, France)

Abstract:

The differentiation of B cells into plasmablasts (PBs) and then plasma cells (PCs) is associated with extensive cell reprogramming and new cell functions. By using specific inhibition strategies (including a novel morpholino RNA antisense approach), we found that early, sustained upregulation of the proviral integrations of Moloney virus 2 (PIM2) kinase is a pivotal event during human B cell *in vitro* differentiation and then continues in mature normal and malignant PCs in the bone marrow. In particular, PIM2 sustained the G1/S transition by acting on CDC25A and p27^{Kip1} and hindering caspase 3-driven apoptosis through BAD phosphorylation and cytoplasmic stabilization of p21^{Cip1}. In PCs, interleukin-6 triggered PIM2 expression, resulting in anti-apoptotic effects on which malignant PCs were particularly dependent. In multiple myeloma, pan-PIM and MCL1 inhibitors displayed synergistic activity. Our results highlight a cell-autonomous function that links kinase activity to the PBs' newly acquired secretion ability and the adaptability observed in both normal and malignant PCs, and finally should prompt the reconsideration of PIM2 as a therapeutic target in multiple myeloma.

Conflict of interest: COI declared - see note

COI notes: M.H., G.C., A.M., L.D., J.M. and T.F. have applied for a European patent on the use of an SSO to modulate PIM2 expression. The other authors have no conflicts of interest to declare.

Preprint server: No;

Author contributions and disclosures: M.H. designed and conducted the experiments, and wrote the paper; G.C. designed the cell differentiation model, and performed cytometry and cell-sorting; F.C. performed genomic analysis; E.A. performed ChIP-qPCR STAT3 experiments; J.D. performed drug combination experiments; A.P. performed single-cell qPCRs; C.D. helped with BACH2 assays and discussed results; S.M. performed CDC25A immunoblotting; G.B. performed FRET experiments; R.V. performed immunostaining; F.L-G. provided bone marrow biopsies; A.M. designed morpholino SSO; O.D. provided multiple myeloma samples; K.T. discussed results; L.D. provided the antisense strategy; J.M. provided cell lines and original data; T.F. designed and supervised the experiments, and wrote the paper.

Non-author contributions and disclosures: No;

Agreement to Share Publication-Related Data and Data Sharing Statement: GEO accession number GSE136990

Clinical trial registration information (if any):

Title: Pivotal role of PIM2 kinase in plasmablast generation and plasma cell survival, opening new treatment options in myeloma

Authors: Marion Haas^{1,2}, Gersende Caron^{1,2}, Fabrice Chatonnet^{1,2}, Stéphane Manenti³, Elina Alaterre⁴, Julie Devin³, Céline Delaloy¹, Giulia Bertolin⁵, Roselyne Viel⁶, Amandine Pignarre^{1,2}, Francisco Llamas-Gutierrez⁷, Anne Marchalot⁸, Olivier Decaux^{1,9}, Karin Tarte^{1,2}, Laurent Delpy⁸, Jérôme Moreaux⁴, and Thierry Fest^{1,2,10}

Affiliations: ¹ Université de Rennes 1, INSERM, Établissement Français du Sang de Bretagne, UMR_S1236, F-35043 Rennes, France; ² Laboratoire d'hématologie et immunologie, Pôle de Biologie, Centre Hospitalier Universitaire, F-35033 Rennes, France; ³ Université de Toulouse, CNRS ERL 5294, INSERM U1037, Centre de Lutte Contre le Cancer (CRCT), F-31000 Toulouse, France; ⁴ Institut de Génétique Humaine, UMR 9002 CNRS-UM ; Pôle de biologie, Centre Hospitalier Universitaire, F-34000 Montpellier; ⁵ Université de Toulouse, CNRS ERL 5294, INSERM U1037, Centre de Lutte Contre le Cancer (CRCT), F-31000 Toulouse, France; ⁶ H2P2 Rennes, France; ⁷ Laboratoire d'Anatomie Pathologique, Pôle de Biologie, Centre Hospitalier Universitaire, F-35033 Rennes, France; ⁸ Université de Limoges, UMR CNRS 7276, INSERM U1262, F-87025 Limoges, France; ⁹ Service d'hématologie clinique, Centre Hospitalier Universitaire, F-35033 Rennes, France; ¹⁰ lead contact.

Correspondence: Thierry Fest, MD, PhD; INSERM U1236, Faculté de Médecine, 2 avenue du Pr Léon Bernard, CS 34317, 35043 Rennes Cedex, France

Phone: +33-299-284-127

Fax: + 33-299-284-152

E-mail : thierry.fest@univ-rennes1.fr

ORCID: <https://orcid.org/0000-0002-6437-4189>

30

Running title: PIM2 kinase and plasma cells

Primary research article

35 Word count (Introduction, Methods, Results and Discussion): 4164

Figure count: 7

Reference count: 52

The manuscript includes Supplemental Information and Supplemental Figures.

Key points

40 B cell commitment into plasmablasts activates *PIM2* via STAT3, which promotes G1/S transition and inhibits caspase 3-driven apoptosis.

Plasma cell survival requires strong expression of *PIM2* & its inhibition exhibits a synergistic effect with MCL1 inhibitor in myeloma.

45

SUMMARY

The differentiation of B cells into plasmablasts (PBs) and then plasma cells (PCs) is associated with extensive cell reprogramming and new cell functions. By using specific inhibition strategies (including a novel morpholino RNA antisense approach), we found
50 that early, sustained upregulation of the proviral integrations of Moloney virus 2 (*PIM2*) kinase is a pivotal event during human B cell *in vitro* differentiation and then continues in mature normal and malignant PCs in the bone marrow. In particular, *PIM2* sustained the G1/S transition by acting on *CDC25A* and *p27^{Kip1}* and hindering caspase 3-driven apoptosis through *BAD* phosphorylation and cytoplasmic stabilization of *p21^{Cip1}*. In
55 PCs, interleukin-6 triggered *PIM2* expression, resulting in anti-apoptotic effects on which malignant PCs were particularly dependent. In multiple myeloma, pan-PIM and MCL1 inhibitors displayed synergistic activity. Our results highlight a cell-autonomous function that links kinase activity to the PBs' newly acquired secretion ability and the adaptability observed in both normal and malignant PCs, and finally should prompt the
60 reconsideration of *PIM2* as a therapeutic target in multiple myeloma.

Keywords: *PIM2* kinase, B cell differentiation, plasma cell, G1/S transition, apoptosis, caspase 3, MCL1, multiple myeloma

65 **INTRODUCTION**

Before becoming plasma cells (PCs), the B cells first pass through an immature, proliferative plasmablast (PB) stage. The PBs emerge after major changes in the B cells' morphology, epigenome-sustained expression profile, and lifespan^{1,2}. This tightly regulated cell metamorphosis can be hijacked by oncogenic alterations that drive malignant transformation. Although there is a large body of data on normal B cell differentiation, studies of B cell malignancies have shown that our understanding of normal B cell function is incomplete³ in particular for identifying specific factors and determining their spatiotemporal involvement in the molecular modifications underlying B cell metamorphosis.

75 We recently reported that the emergence of human PBs is associated with large-scale methylome modifications, with the local acquisition of active epigenetic marks on PC identity genes during a committal step in which some activated B cells differentiate into PBs⁴. These highly proliferative, activated, committed B cells (hereafter referred to as preplasmablasts (prePBs)) are characterized by the silencing of the IL-4/STAT6 pathway and thus downregulation of CD23 surface marker expression⁵. By focusing on this feature, a comparative RNA sequencing (RNA-seq) analysis of prePBs allowed us to identify here a striking increase in expression of the gene encoding the proviral integrations of Moloney virus 2 (PIM2) serine/threonine kinase. The three member of the PIM kinase family are known to phosphorylate numerous substrates involved in crucial cellular functions⁶. Dysregulated expression of PIM kinases has been reported in several cancers including multiple myeloma (MM)^{7,8}. Surprisingly, PIM2 has never been analyzed in the context of normal B cell differentiation. In mouse pro-B cells,

Pim2 expression depends of growth-factor-induced transcription^{9,10}, which justifies further research in the context of PC differentiation.

90 In the present study, we evaluated the effects of PIM2 on PB generation and PC survival. We found that the B cell commitment activates the transcription of *PIM2* in a STAT3-dependent manner, which leads to a strong increase in the protein's expression level and functional activity. We assessed PIM2's biological effects in primary B cells by comparing a normal culture with two conditions in which PIM2's
95 functions were altered by either stopping gene expression or blocking kinase activity. Along with PIM2-mediated BAD phosphorylation, we detected effects on p21^{Cip1}, CDC25A and p27^{Kip1}. During the final step in differentiation, these effects all promote cell survival and entry into the S-phase of the cell cycle. Moreover, PIM2 was found strongly expressed in quiescent mature PCs and essential for cell survival. In
100 malignant setting, PCs are addicted to PIM2 and targeting this kinase was synergistic with BH3-mimetic offering new treatment options for MM.

METHODS

105 **Purification of primary B cells, cell culture, cell cycle assessment, immunophenotyping, cell sorting and protein assays.** Procedures and methods were detailed in Supplemental Methods.

110 **Cell lines culture and viability assays.** Human myeloma cell lines were obtained and cultured as described in¹¹. Viability was assessed for cells treated with selected compounds: AZD1208 & AZD5991 (Selleckchem). CellTiter-Glo® Luminescent Assay kit (Promega) was used as described by the manufacturer. Results were normalized to the samples without treatment and synergy score were calculated using the Bliss method¹² as described in¹³.

115

Primary MM cells. Samples have been collected with the approval of the institutional research board from Rennes university hospital and in accordance with the Declaration of Helsinki. Mononuclear cells were isolated using Ficoll density gradient centrifugation. Samples were cultured in presence of 2 ng/mL IL-6. Cell cytotoxicity was evaluated by flow cytometry by determining the percentage of viable CD138⁺ cells.

125 **SSO experiments.** Inhibition of PIM2 expression is enabled by the use of a vivo-morpholino PIM2 splice-switching antisense oligonucleotide (SSO-PIM2) from Gene Tools, LLC (Philomath, OR, US). An irrelevant vivo-morpholino standard oligonucleotide was used as control (SSO-CTL). PIM2 mRNA knockdown efficiency was evaluated by RT-PCR to simultaneously identify full length (286 pb) and alternatively spliced (176 bp) PIM2 mRNAs on an agarose gel. Quantification of inhibition was also performed by RT-qPCR with exon 2 targeting primers and verified at the protein level by immunoblot.

130

RNA-Sequencing, ATAC-sequencing and data accessibility. Procedures and analysis methods were described in⁵. Raw data are accessible under GEO accession number GSE136990.

135 **RESULTS****The emergence of PIM2 expression during plasmablast commitment**

To identify genes regulated specifically during the final commitment step, we used our previously described *in vitro* differentiation model with human naive B cells (NBCs) generating four cell populations on day (D) 6 (Fig. 1A)¹⁴. The RNA-seq data (confirmed
140 by qPCR assays) revealed a striking elevation of *PIM2* mRNA expression (but not *PIM1* or *PIM3* expression) in prePBs (P2/CD23⁻ population) and PBs (P1 population), relative to B cells diverted from differentiation (P2/CD23⁺ and P3 populations) (Fig. 1B and Fig. S1A). In an unsupervised analysis, the results of single-cell RT-qPCRs in P2/CD23⁻ vs. P2/CD23⁺ cell populations ranked *PIM2* as the most discriminating gene
145 – ahead of *PRDM1* (Fig. 1C and Fig. S1B). Analysis of our RNA-seq datasets showed that *PIM2* was in the top 150 genes characterizing PBs, relative to noncommitted B cell populations (Fig. S1C)⁵. The protein levels correlated perfectly with gene expression levels, with strong *PIM2* expression in prePBs and PBs (Fig. 1B). With regard to human tonsil-derived cell populations, CD19⁺IgD⁻CD38^{bright} PBs expressed
150 higher levels of *PIM2* than other B cell populations (Fig. 1D).

To determine whether *PIM2* gene expression is coupled to genomic changes during PC differentiation, we analyzed our previously published datasets^{4,5} and ENCODE annotations (<https://www.encodeproject.org>). An assay for transposase-accessible chromatin using sequencing (ATAC-seq) showed that the open regions in prePBs and
155 PBs included the *PIM2* promoter and an upstream enhancer. This latter overlaps with a region denoted as interacting physically with the *PIM2* promoter in the FANTOM5 database¹⁵ and with a super-enhancer described in PBs and MM PCs (Fig. 1E)¹⁶. The comparative analysis of genome-wide 5hmC marks in NBCs vs. PBs showed that read

densities increased in both the identified ATAC-seq regions and the body of the *PIM2*
160 sequence; this testified to the enhancer functions and activation in PBs, as has been
shown for PB/PC identity genes (Fig. 1E and Fig. S1D)⁴.

ATAC-seq analysis showed that the time course of promoter opening did not match
the gene expression pattern; this disparity suggests that a transcriptional regulator is
present in the *PIM2* locus (Fig. 1E and Fig. S1D). By chromatin immunoprecipitation
165 (ChIP) sequencing human activated B cells, we identified a BACH2 binding site in the
PIM2 promoter¹⁷. BACH2 inhibition experiments showed a subsequent increase in
PIM2 expression and thus confirmed that BACH2 acts as a repressor (Fig. 1F).
Furthermore, the stimulation of PBs with IL-10, IL-21 and (to a lesser extent) IL-6
resulted in a sharp induction of *PIM2* expression (Fig. 1G). Given that all three
170 cytokines are known to recruit the STAT3 pathway, we exposed the cells to the STAT3
inhibitor C188-9; this led to the dose-dependent repression of *PIM2* expression (Fig.
1G, H). In contrast, IL-2 (which recruits STAT5) and interferon- α were weak inducers
(Fig. 1G). Since STAT3 signaling also induces *PRDM1*/BLIMP1 expression¹⁸, we
wondered if *PIM2* was one of the downstream factors of BLIMP1. In fact, under IL-10
175 (or IL-21, data not shown) stimulation, *PRDM1* was induced but later than *PIM2*
expression (Fig. S1E). In addition, siPRDM1 experiments on primary B cells and U266
MM cells showed no modifications in *PIM2* expression unlike the well-known target
genes of BLIMP1 (Fig S1F-G)^{19,20}, consistent with previous data in prePB/PBs from
knockout *Prdm1* mice²¹. Finally, by ChIP-qPCR on PBs and in RPMI8226 MM cells
180 as well, we confirmed the binding of pSTAT3 on the *PIM2* promoter, as well on the
intron 3 of *PIM2* locus (predicted enhancer region) and in the putative enhancer
located downstream the gene (Fig. 1E and Fig. S1H). Altogether, these results
confirmed that *PIM2* respond directly to STAT3 and not via BLIMP1. Interestingly,

while PIM2-positive PBs were pSTAT3-positive in absence of BACH2, PIM2-
185 negative/BACH2-positive CD23⁺ aBCs were also positive for pSTAT3 suggesting that
the downregulation of BACH2 is required before STAT3 can induce PIM2 expression
(Fig S1I).

Taken as a whole, our results demonstrate that PB differentiation is associated with a
sharp elevation of PIM2 kinase expression; this elevation requires the removal of
190 BACH2 repression and STAT3 activation (Fig. 1J).

PIM2 is required for the differentiation of B cells into PBs

To determine the functional involvement of PIM2 in the committal step and obtain
further differentiated cells on D6, we focused our study on resulting PBs and CD23⁺
195 post-activated B cells (hereafter referred to as CD23⁺ aBCs), which both differed
markedly in their PIM2 expression (Fig. 2A). In subsequent experiments, we compared
a normal culture setting with conditions in which PIM2 was inhibited on D4 by exposure
to the small-molecule pan-PIM inhibitor AZD1208 (hereafter referred as PIMi) or by
specifically blocking *PIM2* gene expression using a novel antisense RNA strategy
200 based on a morpholino splice-switching oligonucleotide (SSO) (Fig. 2B). Cells cultured
with SSO-PIM2 exhibited a dose-dependent decrease in full-length *PIM2* mRNA - the
expression of a weaker band corresponding to alternatively-spliced mRNAs lacking
exon 2 – as well as PIM2 protein expression (Fig. 2C). At the selected dose of 2 μ M,
PIM2 expression was almost completely abrogated in PBs – without affecting *PIM1*
205 expression (Fig. 2D and Fig S2B). While exposure to SSO-PIM2 did not affect the
expression of key transcription factors involved in B cell differentiation (Fig. S2C), PIM2
knockdown led to a sharp decrease in PB generation (Fig. 2E,F and Fig. S2D). In

contrast, CD23⁺ aBCs were not affected. These results suggest that PIM2-kinase activity sustains the PB commitment.

210

PIM2 sustains the G1/S transition through an effect on CDC25A and p27^{Kip1}

A comparison of gene expression in prePBs vs. noncommitted B cell populations evidenced the downregulation of *SMAD3* in the former population. Accordingly, prePBs upregulated *CDC25A*, *CCND2* and *CDK6* expression (Fig. S3A), reentered the cell cycle and gave rise to PBs⁴. At D6, two days after inhibition of PIM2, the S-phase decreased, and cells accumulated in G0/G1 (Fig. 3A and Fig. S3B). In parallel, the number of generated PBs decreased (Fig. 2E-F), regardless of effects on cell death as shown by the QVD-OPH condition (Fig. S3B-C). Moreover, after short exposure to PIMI (12 h) the decrease of S-phase was already observable in absence of effect on apoptosis (Fig. S3B-D). Altogether, these results suggest that PIM2 promotes the G1/S transition independently of the cell death induction. We next performed cell cycle synchronization experiments in the XG21 MM cell line. As expected, unlike the control conditions – in which cells reached the S phase 6 h after release, PIM2 inhibition was associated with blockage of the cells in G1 (Fig. S3E).

225 The phosphatase *CDC25A* is required for the G1/S transition²². *CDC25A* gene expression was significantly greater in PBs than in CD23⁺ aBCs, as well as the protein expression (Fig. 3B). Chemical inhibition of *CDC25A* first led to a dramatic decrease in the proportion of S-phase cells and then, ultimately, to a strong reduction in the number of generated PBs (Fig. S3F,G). Interestingly, PIM2 inhibition led to the decrease of *CDC25A* protein level in PBs without affecting *CDC25A* expression (Fig. 230 3B and Fig. S3H). At D4, the addition of PIMI to cycloheximide-treated cells accelerated

CDC25A's degradation (Fig. 3C and Fig. S3I), while in presence of MG-132, cells maintained CDC25A expression (Fig. 3D).

Cyclin-dependent kinase (CDK) inhibitor 1B (p27^{Kip1}, encoded by the *CDKN1B* gene) prevents progression to G1²³. This effect is linked to p27^{Kip1}'s location in the nucleus; cells that enter the cell cycle show a cyclin D2-mediated nuclear export of p27^{Kip1}²⁴. *CDKN1B* expression was significantly higher in PBs than in CD23⁺ aBCs, while p27^{Kip1} protein expression was lower and mainly located in the nucleus in CD23⁺ aBCs (Fig. 3E). In addition, we detected the threonine 198-phosphorylated (p(Thr198)) form of p27^{Kip1}, predominantly expressed in PBs compared to CD23⁺ aBCs (Fig. 3E). These results prompted us to assess the half-life of p27^{Kip1} in PBs vs. CD23⁺ aBCs. Cycloheximide-treated PBs were more susceptible to p27^{Kip1} proteasome-mediated degradation, as shown after the addition of MG-132 (Fig. 3F,G). Interestingly, in highly proliferative D4 B cells, endogenous immunoprecipitation (IP) of p27^{Kip1} revealed the binding of PIM2, and short treatment by PIMi resulted to a time-dependent decrease of p(Thr198)-p27^{Kip1} (Fig. 3H). PBs generated after PIM2 inhibition showed an increase of the global level of p27^{Kip1} expression - independently to *CDKN1B* expression - particularly in the nucleus (Fig. 3I and Fig. S3J,K). In cycloheximide-treated PBs, the addition of PIMi stabilized p27^{Kip1} (Fig. 3J and Fig S3L). Finally, PIMi-treated PBs showed a decrease of p(Thr198)-p27^{Kip1} as well as a decrease of poly-ubiquitinated forms of p27^{Kip1} in presence of MG-132 (Fig. 3K,L and Fig. S3M).

Overall, PIM2 expression during PB differentiation promotes the G1/S transition in prePBs by stabilizing CDC25A phosphatase and increasing the degradation of cytoplasmic p27^{Kip1} (Fig. 3M).

255

PIM2 hinders the execution of caspase 3-driven apoptosis

The most prominent changes during PB commitment are related to cell death/survival⁴. Indeed, in culture, the majority of B cells were dead on D6 (Fig. 4A). The pan-caspase inhibitor QVD-OPH rescued the cells from death with the exception of the PBs; the latter appeared to be protected from apoptosis, and despite an increase in *CASP3* gene expression (Fig. 4A,B). Investigations of the proteins produced by the various cell subsets in our differentiation model showed that PBs contained higher levels of anti-apoptotic phosphorylated BAD (pBAD) and XIAP (Fig. 4C,D)^{9,10}. Consistent with this finding, IP of PIM2 revealed a binding on BAD most likely required prior to phosphorylation (Fig. 4E). In accordance with this finding and despite the elevation in levels of procaspase 3, PBs displayed low levels of caspase 3 autocatalytic activity and thus did not produce many active p19/p17 forms (as highlighted by lower levels of cleaved PARP) as P2/CD23⁺ cells did (Fig. 4F)²⁵. Overall, PBs maintain caspase 9 in an inactivated state and XIAP protein remains protected from degradation (Fig. 4C-F)²⁶. XIAP is thought to have a key role in PBs by inhibiting caspase 3 activation. Indeed, IP of caspase 3 and XIAP revealed XIAP's binding on p19/p17 fragments of caspase 3 (Fig. 4G), which impairs their catalytic activity on procaspase 3^{27,28}. Lastly, the P2/CD23⁺ cells' complete degradation of PARP (Fig. 4F) showed that terminal B cell differentiation is associated with apoptosis if cells are not otherwise protected by the PB commitment. In PBs, PIM2 inhibition induced an increase in activated caspase 3 levels and thus a decrease in cell viability (Fig. 4H,I and Fig S4A). This effect was driven by (i) the strong mitochondrial depolarization due to the inhibition of pBAD, (ii) the production of cleaved caspase 9, (iii) the decrease in XIAP, (iv) the detection of the p17 fragment of caspase 3, and (v) PARP cleavage (Fig. 4J-L). Lastly, addition of the caspase 3 inhibitor Q-DEVD-OPH rescued the PBs from cell death (Fig. S4B).

Taken as a whole, these data show that PIM2 counteracts the activation of caspase 3 in PBs and thus promotes cell survival.

PIM2 stabilizes cytoplasmic p21^{Cip1} and promotes the latter's binding to caspase

285 **3**

Like p27^{Kip1}, nuclear p21^{Cip1} is a CDK inhibitor and inhibits entry into the S phase of the cell cycle²⁹. PB commitment was associated with a significant increase in transcription of *CDKN1A* (which encodes p21^{Cip1}) and levels of p21^{Cip1} were markedly higher in PBs than in CD23⁺ aBCs (Fig. 5A). Surprisingly, p21^{Cip1} was essentially expressed in the cytoplasm, and endogenous IP experiments yielded a multiprotein complex in which p21^{Cip1} interacted with PIM2 and HSP90 β (Fig. 5B,C). Moreover, PIM2 inhibition led to a dramatic decrease in cytoplasmic p21^{Cip1} without effect on either *CDKN1A* expression or nucleus relocalization (Fig. 5D and Fig. S5A,B). The addition of PIMi to cycloheximide-treated cells accelerated p21^{Cip1}'s degradation (Fig. 5E). Treatment with

290

295

MG-132 induced a strong accumulation of p21^{Cip1}, and the addition of PIMi was associated with elevated poly-ubiquitinated p21^{Cip1} (Fig. 5F,G). XG21 cells presented similar results (Fig. S5C-F). Collectively, these results show that PIM2 stabilizes p21^{Cip1} in PBs by promoting its binding to a cytoplasmic multiprotein complex and thus, prevents p21^{Cip1}'s proteasome-mediated degradation.

300 This PIM2-induced cytoplasmic stabilization of p21^{Cip1} prompted us to question the latter's role in PB commitment. As described previously for other cell types^{30,31}, we hypothesized that p21^{Cip1} interacts with procaspase 3. In fluorescence resonance energy transfer (FRET)³² experiments on XG21 cells, we detected a p21^{Cip1}/procaspase 3 complex whose formation was abrogated by pretreatment of the

305

cells with PIMi (Fig. 5H). IP experiments confirmed the presence of this complex in

PBs (Fig. 5I and Fig. S5G). To determine whether or not p21^{Cip1} mediates apoptosis inhibition, we used siRNA to downregulate *CDKN1A* expression (Fig. S5H). On D6, the generated PBs were found to contain p17-forms of caspase 3 and cleaved PARP - confirming that apoptosis had taken place (Fig. 5J and S5I). Treatment with the small-
310 molecule p21^{Cip1} inhibitor UC2288 was associated with a dose-dependent decrease in cell viability, which was restored by treatment with the caspase 3 inhibitor Q-DEVD-OPH (Fig. 5K and Fig. S5J,K).

Taken as a whole, these findings show that in addition to its mitochondrial effects, PIM2 inhibits the execution of apoptosis by stabilizing cytoplasmic p21^{Cip1}, allowing the latter
315 to bind to procaspase 3, and thus inhibiting the production of activated caspase 3 (Fig. 5L).

Mature plasma cells need PIM2 to inhibit the activation of caspase 3

Plasma cell maturation is a continuum that runs from PBs to fully mature, long-lived
320 PCs such as those residing in the bone marrow (BM) niche, where cell survival depends on various extrinsic factors³³. A comparison of various tonsil-derived B cell populations, PBs, and BM PCs revealed that the level of *PIM2* expression increased along the maturation pathway (Fig. 6A). On paraffin-embedded BM biopsies, staining experiments revealed that virtually all BM PCs – detected either with CD138 or BCMA
325 markers – were strongly positive for PIM2 (Fig. 6B and Fig. S6A,B).

To characterize the regulation and functional contribution of PIM2 in mature PCs, we adapted our cell culture model so that it produced non-proliferating CD138⁺ PCs (Fig. S6C-F), in line with reports on an early PC (ePC) phenotype^{34,35}. As was the case in BM PCs, high levels of PIM2 mRNA and protein expression were observed in ePCs
330 (Fig. 6C). This expression was driven by IL-6 via STAT3 signaling and by the

supernatant from a mesenchymal stromal cell culture (Fig. 6D). As expected, the addition of anti-IL-6 and anti-IL-6R antibodies to the cell culture prevented the induction of PIM2 (Fig. 6D). In this context, we observed clusters of CD138⁺/PIM2⁺ PCs in some areas on BM biopsies, close to CD41-positive megakaryocytes – cells known to
335 produce large amounts of IL-6 and participating to PC BM niche (Fig. 6E)³³.

Treatment of ePCs with PIMi induced an elevation of activated caspase 3 levels, and immunoblot experiments confirmed the increase of mitochondrial depolarization and the execution of apoptosis (Fig. 6F,G). PIMi treatment also led to a significant decrease in p21^{Cip1} levels (Fig. 6G). Interestingly, ePCs (like in some BM PCs) only expressed
340 p21^{Cip1} in the cytoplasm (Fig. 6H and Fig. S6G), and FRET experiments revealed that PIM2 interacted with p21^{Cip1} as well as p21^{Cip1} with caspase 3 (Fig. 6I).

Taken as a whole, our data show that PIM2 is still required in quiescent PCs to protect cells from caspase 3 activation; PIM2 acts at various levels and notably stabilizes cytoplasmic p21^{Cip1}.

345

BH3 mimetics and PIM2 inhibitors have synergistic effects in multiple myeloma

Although PIM2's involvement in MM has been recognized for over a decade, our present findings prompted us to further investigate PIM2's status in malignant PCs. Data from the DepMap Project showed that mRNA expression of *PIM2* (but not of
350 *PIM1*) was elevated in MM cells compared to other tumour cells, whereas CRISPR screening showed a specific high PIM2 dependency score for malignant PCs (Fig. 7A,B and Fig. S7A). BM biopsies from MM patients revealed the intense, widespread expression of PIM2 (Fig. 7C). Data from the University of Arkansas' Total Therapy 2 (TT2) MM cohort showed the strongest *PIM2* expression levels in the high-risk
355 molecular subgroups (Fig. S7B)³⁶. An analysis of data from 765 patients in the

CoMMpass cohort showed that *PIM2* expression was significantly elevated in high-risk cytogenetic subgroups and low in low-risk subgroups (Fig. S7C)^{37,38}. In addition, high *PIM2* expression patients compared to the *PIM2*^{low} group had a worse survival probability (Fig. 7D). This is in line with sc-RNA-seq data on malignant PCs from patients resistant to carfilzomib-daratumumab combination therapy which presented higher *PIM2* expression (Fig. S7D)³⁹. Likewise, we observed a significant increase in *PIM2* expression in cells from an in-house cohort of 14 patients with disease progression soon after first-line treatment (Fig. S7E). Collectively, these data suggest that the severity of MM is associated with *PIM2* expression levels.

Drug resistance is the greatest challenge in MM. It might be possible to overcome this obstacle by acting at the mitochondrial level and lowering the threshold for triggering mitochondrial apoptosis⁴⁰. Venetoclax is reportedly effective in BCL2-translocated MM patients⁴¹. Furthermore, MCL1 is also an attractive target in MM^{41,42} because of its essential effects on PCs survival via inactivation of the pro-apoptotic multidomain of BAX and BAK effectors⁴³. However, in contrast to BCL2 and BCL-xL, MCL1's activity is not antagonized by BAD⁴⁴. Interestingly, data from the TT2 MM cohort showed that the expression levels of MCL1 and *PIM2* are significantly correlated (Fig. S7F). We hypothesized that targeting both *PIM2* and MCL1 might have synergistic effects on mitochondria depolarization because the two proteins act at different levels (Fig. 7E). To this end, we first evaluated the respective effects of PIMi⁴⁵, an MCL1 inhibitor (AZD5991, referred to hereafter as MCL1i)⁴⁶ alone and then when combined. The XG7 and RPMI8226 cell lines were sensitive to MCL1i but the U266 cells were not (Fig. S7G). Low-dose treatment with PIMi greatly enhanced the response to MCL1i in XG7 and RPMI8226 cells (Fig. 7F and Fig. S7H). Interestingly, U266 cells (resistant to PIMi alone and MCL1i alone) became sensitive when the drugs were

combined (Fig. 7G). Lastly, PIMI and MCL1i had synergistic effects on primary MM cells from six patients without effect on CD138⁻ cells (Fig. 7H).

Taken as a whole, these results confirmed that the mitochondrial control of PIM2 is similar in normal and malignant PCs; this finding opens up novel treatment options in
385 MM.

DISCUSSION

The processes by which committed B cells and nascent PBs switch from one molecular program to another had not previously been fully characterized. Here, our experiments
390 with human primary B cells demonstrated that PIM2 kinase is a pivotal factor for the generation and maintenance of PB and PC populations. In particular, our results showed how committed B cells reenter the cell cycle after their proliferation burst, and under subsequently restricted culture conditions, express high levels of PIM2 and thus decrease mitochondrial apoptosis.

395 Our molecular characterization provided strong evidence of the regulation of *PIM2* gene expression and demonstrates *PIM2*'s status as a true PC-identity gene recruited at the same time as *PRDM1* and *IRF4*, once BACH2 repression has been released. In prePBs and PBs, both IL-10 and IL-21 cytokines drive PIM2 expression via pSTAT3 signaling and (in PCs) by IL-6, which establishes a direct link between growth-factor-
400 induced transcription and a kinase-dependent pathway that promotes survival and cell cycle reentry.

The cell cycle provides windows of opportunity for chromatin remodeling and thus gene activation⁴⁷. Committed B cells increase their expression of *CDC25A* and in parallel PIM2 helps to stabilize the *CDC25A* protein and thus prompts cells to enter the S phase
405 and progress to the PB state independently of effects on apoptosis²². Interestingly, PIM2's promotion of cell cycle is accentuated by the degradation of cytoplasmic p27^{Kip1}, which prevents the latter from accumulating or returning to the nucleus. Indeed, PIM2's effect on p27^{Kip1} is mediated by the phosphorylation of threonine 198 residue, consistent with the known cytoplasmic localization of p(Thr198)-p27^{Kip1} and
410 its binding to 14-3-3 leading to its proteasomal degradation⁴⁸. In contrast, in PCs, p27^{Kip1} accumulated in the nucleus - independently of high PIM2 expression - to halt the cell cycle and so without being degraded by cytoplasmic PIM2.

Caspases 9 and 3 become resistant to activation by apoptotic stimuli when B cells differentiate into PBs, and the apoptosis of short-lived PCs *in vitro* and *in vivo* is largely
415 independent of the key apoptotic caspases⁴⁹. Our present results provide insights into the mechanisms whereby B cell death is avoided - despite intense expression of cell death-related genes in committed cells⁴ - allowing PB generation and survival. Production of pBAD helps to maintain the integrity of mitochondria, as evidenced by increased XIAP expression and the overall inhibition of caspase 3 self-activation.
420 Knockdown and dose-dependent experiments have shown that this mitochondrial adaptation is mediated and made possible by high levels of PIM2 expression and its binding activity to BAD; this is in line with data from constitutive PIM2 expression models, with the detection of pBAD, its binding to 14-3-3, and inhibition of BAD/BCL-XL binding^{10,50}.

425 One of the ways in which PIM2 regulates apoptosis during the differentiation of B cells into PBs involves restricting p21^{Cip1} to the cytoplasm. During this step, cells progress

from G1 to S and proliferate; hence, the cytoplasmic expression of p21^{Cip1} makes sense because its presence in the nucleus blocks cells in G1⁵¹. However, further investigations on quiescent PC populations demonstrate that p21^{Cip1} stays in the cytoplasm which sheds light on its pleotropic functions. In PBs, PIM2 stabilizes cytoplasmic p21^{Cip1} by promoting the formation of a complex with HSP90 β and thus reducing the proteasomal degradation of p21^{Cip1}. Interestingly, p21^{Cip1} also binds to procaspase 3 in a PIM2-dependent manner and FRET experiments showed that the addition of PIMi abrogated p21^{Cip1}'s binding to procaspase 3. In PBs, PIM2 acts by promoting the formation of a multiprotein complex which inhibits the caspase 3 activation. This effect complements the production of pBAD and the inhibition of mitochondrial depolarization and shows that PIM2 acts in several ways to ensure the survival of PBs.

Entry into cell cycle quiescence accompanies the final phenotypic maturation of PCs and requires CDK inhibitors regulated by IL-6⁵². By modifying the culture conditions, we obtained fully mature PCs that strongly expressed PIM2 and absolutely required IL-6. At the cellular level, PIM2's anti-apoptotic effects were characterized by maintenance of mitochondrial integrity and promotion of caspase 3/p21^{Cip1} binding. Although it is now accepted that viability is not an intrinsic property of BM PCs but is conferred on the cells by their immediate environment⁵³, our present observations of marked expression of PIM2 in BM PCs suggest that this kinase has a crucial role in long-term cell survival and might be involved in the functional activity of the PC niche through IL-6-dependent crosstalk between the cell and its microenvironment⁵⁴.

Our results revealed a hitherto unexpected role of PIM2 kinase in terminal B cell differentiation and, more generally, the PC's biology. PIM2 kinase's pleotropic effects

enable the cell to modify its regulation of apoptosis and to promote survival when faced with protein secretion overload. The data from the DepMap Project show that malignant PCs are “addicted” to PIM2, and elevated PIM2 expression in the most severe cases of MM suggests that PIM2 is linked to clinical severity. Small-molecule inhibitors of PIM
455 have given some encouraging results in preclinical models, and recently in MM patients with relapsed and/or refractory disease⁵⁵. Indeed, and despite a relative low objective response rate (partial response or better), patients who reached the recommended dose of treatment, PIM447 drug demonstrated a single-agent antitumor activity with a significant improvement of the median progression-free survival and the
460 rate of clinical benefit. However, bone marrow examination of patients failed to reveal a clinically significant reduction in malignant PCs suggesting that PIM447 exerted antitumor responses via cytostatic rather than apoptotic mechanisms⁵⁵. Taking into account that MM tumor cells increase their dependence on MCL1 during the course of the disease⁴¹, we could speculate that MCL1 could counteract the induction of cell
465 death by PIMi. In the context of the PIM447 clinical trial⁵⁵, antiproliferative effects could appear at low doses while cell death would require dose escalation – possibly with unacceptable toxicities – to counterbalance MCL1-dependency. Given that MCL1’s action on the mitochondrial membrane is independent of BAD, dual pharmacological inhibition of PIM2 and MCL1 is highly synergistic; low doses of PIMi significantly
470 increased the efficacy of the anti-MCL1 drug. Interestingly, this drug combination can reverse U266 cell’s primary resistance to MCL1i and PIMi.

In conclusion, our present results showed that the final transcriptional modifications in B cells committed to differentiation into PBs are associated with the expression of a
475 set of crucial genes, including *PIM2*. The newly established adaptive status of the

generated PBs is maintained in mature PCs. Lastly, we showed that PIM2 kinase's anti-apoptotic effects should be further investigated in the context of novel treatment strategies in MM.

480 **ACKNOWLEDGMENTS**

This work was funded by an internal grant from the Hematology Laboratory, CHU de Rennes, and Région GO Ligue contre le Cancer. MH has received a doctoral fellowship from FHU CAMIn, Ligue Contre le Cancer/Comité d'Ille et Vilaine. AP received a PhD fellowship from Région Bretagne and Ligue Nationale contre le Cancer.

485 Immunofluorescence studies were performed at the Microscopy Rennes Imaging Center (MRic-ALMF) and in the H2P2 facility, both of which are members of the UMS 6480 Biosit (Rennes, France) and the French national France-BioImaging infrastructure network funded by the French Research Agency (ANR-10-INBS-04). Cell sorting was performed at the Biosit Flow Cytometry and the CytomeTRI cell sorting
490 facilities (UMS6480 Biosit). We are indebted to the Centre de Ressources Biologiques (CRB)-Santé (BB-0033-00056, <http://www.crbsante-rennes.com>) at Rennes University Medical Center for its help with processing biological samples, and we also thank several clinicians and patients for providing samples for research purposes. We thank the MMRF for sharing the RNA sequencing and clinical data for patients enrolled in the
495 CoMMpass study via the MMRF genomics portal.

AUTHOR CONTRIBUTIONS

M.H. designed and conducted the experiments, and wrote the paper; G.C. designed the cell differentiation model, and performed cytometry and cell-sorting; F.C. performed
500 genomic analysis; E.A performed ChIP-qPCR STAT3 experiments; J.D. performed

drug combination experiments; A.P. performed single-cell qPCRs; C.D. helped with BACH2 assays and discussed results; S.M. performed CDC25A immunoblotting; G.B. performed FRET experiments; R.V. performed immunostaining; F.L-G. provided bone marrow biopsies; A.M. designed morpholino SSO; O.D. provided multiple myeloma
505 samples; K.T. discussed results; L.D. provided the antisense strategy; J.M. provided cell lines and original data; T.F. designed and supervised the experiments, and wrote the paper.

COMPETING INTERESTS

510 M.H., G.C., A.M., L.D., J.M. and T.F. have applied for a European patent on the use of an SSO to modulate PIM2 expression. The other authors have no conflicts of interest to declare.

515

REFERENCES

1. Fairfax KA, Kallies A, Nutt SL, Tarlinton DM. Plasma cell development: From B-cell subsets to long-term survival niches. *Seminars in Immunology*. 2008;20(1):49–58.
- 520 2. Willis SN, Nutt SL. New players in the gene regulatory network controlling late B cell differentiation. *Current Opinion in Immunology*. 2019;58:68–74.
3. Shaffer AL, Young RM, Staudt LM. Pathogenesis of Human B Cell Lymphomas. *Annu Rev Immunol*. 2012;30(1):565–610.
- 525 4. Caron G, Hussein M, Kulis M, et al. Cell-Cycle-Dependent Reconfiguration of the DNA Methylome during Terminal Differentiation of Human B Cells into Plasma Cells. *Cell Reports*. 2015;13(5):1059–1071.
5. Pignarre A, Chatonnet F, Caron G, et al. Plasmablasts derive from CD23– activated B cells after the extinction of IL-4/STAT6 signaling and IRF4 induction. *Blood*. 2021;137(9):1166–1180.
- 530 6. Mondello P, Cuzzocrea S, Mian M. Pim kinases in hematological malignancies: where are we now and where are we going? *J Hematol Oncol*. 2014;7:95–103.
7. Keane NA, Reidy M, Natoni A, Raab MS, O'Dwyer M. Targeting the Pim kinases in multiple myeloma. *Blood Cancer Journal*. 2015;5(7):e325–e325.
8. Panchal NK, Sabina EP. A serine/threonine protein PIM kinase as a biomarker of cancer and a target for anti-tumor therapy. *Life Sciences*. 2020;255:117866.
- 535 9. Fox CJ. The serine/threonine kinase Pim-2 is a transcriptionally regulated apoptotic inhibitor. *Genes Dev*. 2003;17(15):1841–1854.
10. Yan B, Zemskova M, Holder S, et al. The PIM-2 Kinase Phosphorylates BAD on Serine 112 and Reverses BAD-induced Cell Death. *J Biol Chem*. 2003;278(46):45358–45367.
- 540 11. Moreaux J, Klein B, Bataille R, et al. A high-risk signature for patients with multiple myeloma established from the molecular classification of human myeloma cell lines. *Haematologica*. 2011;96(4):574–582.
12. Greco WR, Bravo G, Parsons JC. The search for synergy: a critical review from a response surface perspective. *Pharmacol Rev*. 1995;47(2):331.
- 545 13. Combès E, Andrade AF, Tosi D, et al. Inhibition of Ataxia-Telangiectasia Mutated and RAD3-Related (ATR) Overcomes Oxaliplatin Resistance and Promotes Antitumor Immunity in Colorectal Cancer. *Cancer Res*. 2019;79(11):2933–2946.
14. Le Gallou S, Caron G, Delaloy C, et al. IL-2 Requirement for Human Plasma Cell Generation: Coupling Differentiation and Proliferation by Enhancing MAPK-ERK

- 550 Signaling. *J Immunol.* 2012;189(1):161–173.
- 15.Andersson R, Gebhard C, Miguel-Escalada I, et al. An atlas of active enhancers across human cell types and tissues. *Nature.* 2014;507(7493):455–461.
- 16.Hnisz D, Abraham BJ, Lee TI, et al. Super-Enhancers in the Control of Cell Identity and Disease. *Cell.* 2013;155(4):934–947.
- 555 17.Hipp N, Symington H, Pastoret C, et al. IL-2 imprints human naive B cell fate towards plasma cell through ERK/ELK1-mediated BACH2 repression. *Nat Commun.* 2017;8(1):1443–1426.
- 18.Ozaki K, Spolski R, Ettinger R, et al. Regulation of B Cell Differentiation and Plasma Cell Generation by IL-21, a Novel Inducer of Blimp-1 and Bcl-6. *J Immunol.* 2004;173(9):5361–5371.
- 560 19.Doody GM, Care MA, Burgoyne NJ, et al. An extended set of PRDM1/BLIMP1 target genes links binding motif type to dynamic repression. *Nucleic Acids Research.* 2010;38(16):5336–5350.
- 20.Shaffer AL, Lin K-I, Kuo TC, et al. Blimp-1 Orchestrates Plasma Cell Differentiation by Extinguishing the Mature B Cell Gene Expression Program. *Immunity.* 2002;17(1):51–62.
- 565 21.Minnich M, Tagoh H, Bönelt P, et al. Multifunctional role of the transcription factor Blimp-1 in coordinating plasma cell differentiation. *Nat Immunol.* 2016;17(3):331–343.
- 22.Hoffmann I, Draetta G, Karsenti E. Activation of the phosphatase activity of human cdc25A by a cdk2-cyclin E dependent phosphorylation at the G1/S transition. *Embo J.* 1994;13(18):4302–4310.
- 570 23.Abbastabar M, Kheyrollah M, Azizian K, et al. Multiple functions of p27 in cell cycle, apoptosis, epigenetic modification and transcriptional regulation for the control of cell growth: A double-edged sword protein. *DNA Repair.* 2018;69:63–72.
- 575 24.Susaki E, Nakayama K, Nakayama KI. Cyclin D2 Translocates p27 out of the Nucleus and Promotes Its Degradation at the G0-G1 Transition. *Mol Cell Biol.* 2007;27(13):4626–4640.
- 25.Ponder KG, Boise LH. The prodomain of caspase-3 regulates its own removal and caspase activation. *Cell Death Disc.* 2019;5(1):56–66.
- 580 26.Datta SR, Ranger AM, Lin MZ, et al. Survival Factor-Mediated BAD Phosphorylation Raises the Mitochondrial Threshold for Apoptosis. *Dev Cell.* 2002;3(5):631–643.
- 27.Riedl SJ, Renatus M, Schwarzenbacher R, et al. Structural Basis for the Inhibition of Caspase-3 by XIAP. *Cell.* 2001;104:791–800.

- 585 28.Suzuki Y, Nakabayashi Y, Nakata K, Reed JC, Takahashi R. X-linked Inhibitor of Apoptosis Protein (XIAP) Inhibits Caspase-3 and -7 in Distinct Modes. *J Biol Chem.* 2001;276(29):27058–27063.
- 29.Elledge SJ, Hardy CFJ, Pautz A, et al. Cell Cycle Checkpoints: Preventing an Identity Crisis. *Science.* 1996;274(5293):1964–1972.
- 590 30.Asada M. Apoptosis inhibitory activity of cytoplasmic p21Cip1/WAF1 in monocytic differentiation. *Embo J.* 1999;18(5):1223–1234.
- 31.Suzuki A, Kawano H, Hayashida M, et al. Procaspase 3/p21 complex formation to resist Fas-mediated cell death is initiated as a result of the phosphorylation of p21 by protein kinase A. *Cell Death Differ.* 2000;7(8):721–728.
- 595 32.Bertolin G, Sizaire F, Déméautis C, et al. Optimized FRET Pairs and Quantification Approaches To Detect the Activation of Aurora Kinase A at Mitosis. *ACS Sens.* 2019;4(8):2018–2027.
- 33.Winter O, Moser K, Mohr E, et al. Megakaryocytes constitute a functional component of a plasma cell niche in the bone marrow. *Blood.* 2010;116(11):1867–1875.
- 600 34.Kassambara A, Rème T, Jourdan M, et al. GenomicScape: An Easy-to-Use Web Tool for Gene Expression Data Analysis. Application to Investigate the Molecular Events in the Differentiation of B Cells into Plasma Cells. *PLoS Comput Biol.* 2015;11(1):e1004077.
- 605 35.Nutt SL, Hodgkin PD, Tarlinton DM, Corcoran LM. The generation of antibody-secreting plasma cells. *Nat Rev Immunol.* 2015;15(3):160–171.
- 36.Zhan F, Huang Y, Colla S, et al. The molecular classification of multiple myeloma. *Blood.* 2006;108(6):2020–2028.
- 610 37.Bergsagel PL, Mateos M-V, Gutierrez NC, Rajkumar SV, San Miguel JF. Improving overall survival and overcoming adverse prognosis in the treatment of cytogenetically high-risk multiple myeloma. *Blood.* 2013;121(6):884–892.
- 38.Perrot A, Lauwers-Cances V, Tournay E, et al. Development and Validation of a Cytogenetic Prognostic Index Predicting Survival in Multiple Myeloma. *J Clin Oncol.* 2019;37(19):1657–1665.
- 615 39.Cohen YC, Zada M, Wang S-Y, et al. Identification of resistance pathways and therapeutic targets in relapsed multiple myeloma patients through single-cell sequencing. *Nat Med.* 2021;27(3):491–503.
- 40.Gimenez-Bonafe P, Tortosa A, Perez-Tomas R. Overcoming Drug Resistance by Enhancing Apoptosis of Tumor Cells. *Current Cancer Drug Targets.* 2009;9(3):320–

340.

- 620 41. Gomez-Bougie P, Maiga S, Tessoulin B, et al. BH3-mimetic toolkit guides the respective use of BCL2 and MCL1 BH3-mimetics in myeloma treatment. *Blood*. 2018;132(25):2656–2669.
42. Slomp A, Moesbergen LM, Gong J, et al. Multiple myeloma with 1q21 amplification is highly sensitive to MCL-1 targeting. *Blood Advances*. 2019;3(24):4202–4214.
- 625 43. Peperzak V, Vikström I, Walker J, et al. Mcl-1 is essential for the survival of plasma cells. *Nat Immunol*. 2013;14(3):10.
44. Wei AH, Roberts AW, Spencer A, et al. Targeting MCL-1 in hematologic malignancies: Rationale and progress. *Blood Reviews*. 2020;44:100672.
- 630 45. Keeton EK, McEachern K, Dillman KS, et al. AZD1208, a potent and selective pan-Pim kinase inhibitor, demonstrates efficacy in preclinical models of acute myeloid leukemia. *Blood*. 2014;123(6):905–913.
46. Tron AE, Belmonte MA, Adam A, et al. Discovery of Mcl-1-specific inhibitor AZD5991 and preclinical activity in multiple myeloma and acute myeloid leukemia. *Nat Commun*. 2018;9(1):5341.
- 635 47. Pop R, Shearstone JR, Shen Q, et al. A Key Commitment Step in Erythropoiesis Is Synchronized with the Cell Cycle Clock through Mutual Inhibition between PU.1 and S-Phase Progression. *PLoS Biol*. 2010;8(9):e1000484.
- 640 48. Fujita N, Sato S, Katayama K, Tsuruo T. Akt-dependent Phosphorylation of p27Kip1 Promotes Binding to 14-3-3 and Cytoplasmic Localization. *Journal of Biological Chemistry*. 2002;277(32):28706–28713.
49. Auner HW, Beham-Schmid C, Dillon N, Sabbattini P. The life span of short-lived plasma cells is partly determined by a block on activation of apoptotic caspases acting in combination with endoplasmic reticulum stress. *Blood*. 2010;116(18):3445–3455.
- 645 50. Macdonald A, Campbell DG, Toth R, et al. Pim kinases phosphorylate multiple sites on Bad and promote 14-3-3 binding and dissociation from Bcl-XL. *BMC Cell Biology*. 2006;7:1–14.
51. Kreis, Louwen, Yuan. The Multifaceted p21 (Cip1/Waf1/CDKN1A) in Cell Differentiation, Migration and Cancer Therapy. *Cancers*. 2019;11(9):1220.
- 650 52. Tourigny MR, Ursini-Siegel J, Lee H, et al. CDK Inhibitor p18INK4c Is Required for the Generation of Functional Plasma Cells. *Immunity*. 2002;17(2):179–189.
53. Sze DM-Y, Toellner K-M, de Vries CG, Taylor DR, MacLennan ICM. Intrinsic Constraint on Plasmablast Growth and Extrinsic Limits of Plasma Cell Survival. *J Exp Med*. 2000;192(6):813–822.

- 655 54. Wols HAM, Underhill GH, Kansas GS, Witte PL. The Role of Bone Marrow-Derived Stromal Cells in the Maintenance of Plasma Cell Longevity. *J Immunol.* 2002;169(8):4213–4221.
55. Raab MS, Thomas SK, Ocio EM, et al. The first-in-human study of the pan-PIM kinase inhibitor PIM447 in patients with relapsed and/or refractory multiple myeloma. *Leukemia.* 2019;33(12):2924–2933.
- 660 56. Marchalot A, Lambert J-M, Boyer F, et al. Splice switching oligonucleotide mediated gene knockdown in B cells and plasma cells. *BioRxiv preprint.* 2020;
57. Zammarchi F, de Stanchina E, Bournazou E, et al. Antitumorigenic potential of STAT3 alternative splicing modulation. *Proc Natl Acad Sci USA.* 2011;108(43):17779–17784.

665

FIGURE LEGENDS

Fig 1. *PIM2* expression and regulation during normal B cell differentiation

A. Using a two-step cell culture process, VPD-labeled NBCs were differentiated into
670 the cell populations P1, P2 and P3. P2 cells were subdivided into P2/CD23⁺ and
P2/CD23⁻ subsets. The plasmablast P1 population arose from the P2/CD23⁻ subset.

B. Left, *PIM2* RNA-seq results on D4 or D5 in the various cell populations. Data are
quoted as the mean \pm SD, n=3. **Right,** *PIM2* mRNA expression in the various cell
populations on D6. mRNA data are quoted as the median (range), n=6. **Bottom,** *PIM2*
675 protein expression in all cell populations, from D0 to D6.

C. A single-cell qRT-PCR heatmap of the expression of 31 genes in P2/CD23⁻ vs.
P2/CD23⁺ cell subsets; red arrow indicates *PIM2* mRNA expression.

D. *PIM2* mRNA expression (top) and protein expression (bottom) in different tonsil-
derived B cell populations. mRNA data are quoted as the median (range), n=7.

680 **E.** The Integrative Genomic Viewer (IGV) genome browser window, showing several
features around the *PIM2* locus. Colored tracks at the top are our RNA-seq and ATAC-
seq data⁵. ATAC-seq showed that the open regions included the *PIM2* promoter and
an upstream enhancer which physically interact together. ATAC-seq regions close to
PIM2 comprise transcription factor binding sites (TFBS) for relevant factors such as
685 STAT3, according to ENCODE data, and also BACH2, including one we have
identified by chromatin immunoprecipitation¹⁷. 5hmC marks are identified in ATAC-
seq regions and the body of the *PIM2* sequence in PBs⁴. For details, see Fig. S2a.

F. Levels of *BACH2* and *PIM2* mRNA expression (left) and protein expression (right)
in D4^{lo} cells after transfection with siBACH2 on D2. mRNA data are quoted as the
690 mean \pm SD, n=4.

G. On D5, PBs were sorted, starved and then stimulated with the indicated cytokines. **Left**, *PIM2* mRNA expression after 4 h (white) and 16 h (black). For each time point, the results were normalized against the non-stimulated condition (set arbitrarily to 1, in grey). mRNA data are quoted as the mean \pm SD, n=5. **Right**, *PIM2*, pSTAT3 and pSTAT5 protein expression after 16 h.

H. On D5, PBs were sorted, starved and then treated with increasing doses of a STAT3 inhibitor 1 h before the addition of IL-10. *PIM2* mRNA expression (left) and protein expression (right) were assessed 4 h after the addition of IL-10. mRNA data are quoted as the mean \pm SD, n=5.

J. Regulation of *PIM2* expression during B cell differentiation. At the start of B cell differentiation and despite the open chromatin on the promoter and on other regulatory regions, *PIM2* expression is constrained by BACH2. BACH2 expression then declines throughout the differentiation process, while T follicular helper (Tfh)-driven molecules stimulate STAT3 signaling. Both events promote the burst in *PIM2* expression in cells committed to differentiation into PBs.

C, F, G, H, Statistical significance was evaluated using Mann-Whitney (**C, F, G, H**) or Kruskal-Wallis (**H**) test. * $P < 0.05$, ** $P < 0.01$, *** $P < 0.001$.

See also Fig. S1.

710 **Fig 2. Specific inhibition of PIM2 affects the generation of plasmablasts**

A. Left, On D6, total blood B cells were differentiated into two different cell populations: CD23+ aBCs and PBs. **Right**, *PIM2* mRNA expression and protein expression in CD23+ aBCs and PBs on D6. Data are quoted as the median (range), n=10.

715 **B.** Diagram illustrating the SSO-PIM2's mode of action. Specific inhibition of *PIM2*

was performed by specifically blocking *PIM2* gene expression using a novel antisense RNA strategy based on a morpholino splice-switching oligonucleotide (SSO). In line with a previously described forced-splicing-dependent nonsense-mediated decay approach to knockdown^{56,57}, the SSO targets the 5' splice site of *PIM2*'s exon 2, induces out-of-frame exon skipping, and generates a premature stop codon in exon 4. This latter eventually triggers nonsense-mediated decay or generates a truncated, non-functional protein. See the Supplemental Material & Methods for details.

C. Activated B cells were treated with various doses of SSO-*PIM2* from D4 to D6.

Top, *PIM2* mRNA expression levels were compared with those in a control experiment, set arbitrarily to 100% (mean \pm SD, n=4) (top). The agarose gel from the *PIM2* PCR shows the exon skipping (bottom). Dose escalation experiments allow us to select an SSO-*PIM2* concentration of 2 μ M for our subsequent experiments in our in vitro model. **Bottom**, *PIM2* protein expression was assessed by western blot on D6 after *PIM2* inhibition with increasing dose of SSO-*PIM2*.

D. *PIM2* mRNA expression (mean \pm SD, n=6) (left) and protein expression (right), as determined by immunoblotting and immunofluorescence in CD23⁺ aBCs and PBs after *PIM2* inhibition with SSO-*PIM2* (2 μ M). Sytox (blue) stains the nucleus. Scale bar: 10 μ m.

E-F. On D4, cells were treated with SSO-*PIM2* (**E**) or increasing doses of *PIMi* (**F**). On D6, analysis of cell differentiation was performed in the model described in Fig. 2A. Proportion of CD23⁺ aBCs (CD23⁺/CD38^{low} cells) and PBs (CD38^{high}/CD23⁻ cells), and the absolute number of each cell population were assessed by flow cytometry according to the gating strategy described in Fig. S2D". **Left**, the absolute number of PBs and CD23⁺ aBCs obtained on D6 after *PIM2* inhibition, compared with controls. Data are quoted as the mean \pm SD, n=8. **Right**, one representative result of

the proportion of PBs on D6 (evaluated using flow cytometry) after PIM2 inhibition, compared with controls.

A, E, F, Statistical significance was evaluated using Mann-Whitney (**A**), Wilcoxon (**E**) and Friedman (**F**) tests. * $P < 0.05$, ** $P < 0.01$, *** $P < 0.001$, **** $P < 0.0001$.

745 See also Fig. S2.

Fig 3. PIM2 supports cell cycle entry by promoting the G1/S transition

A. Flow cytometry evaluation of the cell cycle in PBs on D6 after treatment with SSO-PIM2 and increasing doses of PIMi, compared with controls (n=6).

750 **B. Left**, *CDC25A* mRNA expression in CD23+ aBCs and PBs on D6. Data are quoted as the median (range), n=10. **Right**, *CDC25A* protein expression (in the red square) in CD23+ aBCs and PBs on D6 after treatment with PIMi . *) *non-specific band*.

C. D4 B cells were treated with PIMi and incubated with cycloheximide (CHX). At the indicated time points, *CDC25A* expression was analyzed by immunoblotting.

755 **D**. On D4, B cells were treated with PIMi and incubated in presence of MG-132 for 2 h. *CDC25A* expression was analyzed by immunoblotting.

E. Left, *CDKN1B* mRNA expression in CD23+ aBCs and PBs on D6. Data are quoted as the median (range), n=10. **Right**, PIM2, p(Thr198)-p27^{Kip1} (p-p27) and total p27^{Kip1} protein expression in CD23+ aBCs and PBs on D6 in total protein extracts and nuclear

760 & cytoplasmic fractions.

F. Cells were incubated with cycloheximide (CHX) on D6, just before sorting. At the indicated time points, p27^{Kip1} expression in CD23+ aBCs and PBs was analyzed by immunoblotting.

G. Cells were incubated for 4 h with MG-132 before sorting on D6. p27^{Kip1} expression
765 in CD23+ aBCs and PBs was assessed by immunoblotting.

H. Left, Immunoprecipitation of p27^{Kip1} in D4-activated B cells. PIM2 and p27^{Kip1} were detected by immunoblotting. **Right**, On D4, activated B cells were shortly treated with PIMi. At the indicated time points, p(Thr198)-p27^{Kip1} (p-p27) and total p27^{Kip1} protein expression were assessed by immunoblotting.

770 **I.** PIM2 and p27^{Kip1} protein expression in PBs after treatment with PIMi in total protein extracts and nuclear & cytoplasmic fractions.

J. On D6, cells were treated with PIMi and incubated with CHX before sorting. At the indicated time points, p27^{Kip1} expression in PBs was assessed by immunoblotting.

K. On D6, cells were treated with PIMi for 2 h before sorting. p(Thr198)-p27^{Kip1} (p-p27) and total p27^{Kip1} were assessed by immunoblotting.

L. On D6, cells were incubated in presence or absence of PIMi for 2 h before addition (or not) of MG-132 for 4 h. **Left**, p27^{Kip1} was assessed by immunoblotting. **Right**, Polyubiquitinated p27^{Kip1} and native p27^{Kip1} were assessed by immunoblotting.

M. PIM2 promotes the G1/S transition. Positive effects (in pink) are PIM2-dependent, while effects not directly related to PIM2 are shown in green. On one hand, PIM2 induces p27^{Kip1} degradation once the protein is localized in the cytoplasm. On the other hand, PIM2 maintains the expression of CDC25A.

A, B, E, Statistical significance was evaluated using Kruskal-Wallis (**A**, for PIMi experiment) and Mann-Whitney (**A**, for SSO experiment, **B, E**) tests. * $P < 0.05$, ** $P < 0.01$, *** $P < 0.001$, **** $P < 0.0001$, ns = not significant.

See also Fig. S3.

Fig 4. PIM2 is required to counter mitochondrial apoptosis.

A. Analysis of cell death was performed in the model previously described in⁵. Cell viability (number of caspase-3-active negative (alive cells) and positive (death cells))

and cell differentiation (number of P3 cells, P2/CD23+ cells, P2/CD23- cells and P1 cells) was assessed by flow cytometry. **Left**, the total numbers of dead cells and living cells in the four populations on D6. The pie chart shows the percentage of cells, n=7.

Right, on D4, cells were treated (or not) with QVD-OPH. On D6, the numbers of cells
795 in each population were recorded. Data are quoted as the mean \pm SD, n=6.

B. CASP3 mRNA expression in the various cell populations on D6. The data are quoted as the median (range), n=6.

C. Factors in the mitochondrial apoptosis pathway involved in B cell differentiation. The green "+" symbol represents a death-activating effect, while the red "-" symbol
800 represents a death-inhibiting effect. The pro-apoptotic protein BAD causes depolarization of the mitochondria, followed by the cleavage of procaspase 9 into active caspase 9 which in turn cleaves procaspase 3 to generate an intermediate, inactive p20 form. Following an auto-catalytic process, the p20 form gives rise to catalytically active p19 and p17 fragments. These molecules cleave PARP (the end
805 effector in the apoptotic process) and also p20 in a feedback loop. Molecules are released from the mitochondria following depolarization and block the action of the inhibitor of apoptosis proteins, including XIAP. The phosphorylation of BAD leads to its cytoplasmic sequestration by 14-3-3, thus hijacking its pro-apoptotic effect.

D, F. Assessment of the protein expression of factors involved in the mitochondrial
810 apoptosis pathway during primary B cell differentiation. "*Cl*" for *cleaved*.

E. Immunoprecipitation of PIM2 in PBs. PIM2 and BAD were detected by immunoblotting.

G. Immunoprecipitation of XIAP (top) and caspase 3 (bottom) in PBs. XIAP and caspase 3 were detected by immunoblotting.

815 **H-I.** Flow cytometry evaluation of the percentage of active-caspase-3-positive PBs on

D6, after treatment with SSO-PIM2 (**H**) or with increasing doses of PIMi (**I**), relative to controls. Data are quoted as the mean \pm SD, n=8.

820 **J.** One representative result of the TMRM signal on D6 in PBs (analyzed by flow cytometry) after treatment with SSO-PIM2 (left) or PIMi (right), compared with controls.

K-L. Assessment of protein expression levels in PBs on D6 for factors involved in the mitochondrial apoptosis pathway after PIM2 inhibition by SSO-PIM2 (**K**) or PIMi (10 μ M) (**L**), compared with controls.

825 **A, B, H, I,** Statistical significance was evaluated using Mann-Whitney (**A, B**), Wilcoxon (**H**) and Friedman (**I**) tests. * $P < 0.05$, ** $P < 0.01$, *** $P < 0.001$, **** $P < 0.0001$, ns = not significant.

See also Fig. S4.

Fig 5. PIM2 helps to stabilize cytoplasmic p21^{Cip1} and promotes the caspase
830 **3/p21^{Cip1} interaction**

A. Left, *CDKN1A* mRNA expression was measured on D6 in CD23+ aBCs and PBs. Data are quoted as the median (range), n=10. **Right,** PIM2 and p21^{Cip1} protein expression on D6 in CD23+ aBCs and PBs.

835 **B.** PIM2 and p21^{Cip1} protein expression was measured in nuclear & cytoplasmic fractions from CD23+ aBCs and PBs.

C. PIM2 (left) and p21^{Cip1} (right) immunoprecipitation in PBs. HSP90 β , p21^{Cip1} and PIM2 were detected by immunoblotting.

D. PIM2 and p21^{Cip1} protein expression after treatment with SSO-PIM2 (top) or PIMi (bottom) in total extracts from PBs.

840 **E.** PBs were sorted and then treated with PIMi and incubated with CHX. At indicated

times, p21^{Cip1} expression was assessed by immunoblotting.

F. PBs were sorted and then treated with PIMi for 2 h in presence (or not) of MG-132. p21^{Cip1} was assessed by immunoblotting.

G. PBs were treated 30 min with PIMi after incubation in the presence of MG-132 for
845 2 h. Polyubiquitinated p21^{Cip1} and native p21^{Cip1} were assessed by immunoblotting.

H. FRET/FLIM was analyzed in XG21 cells stained for caspase 3 (the donor) in the presence or absence of p21^{Cip1} (the acceptor). Cells were left untreated (upper panel) or treated with PIMi (lower panel). The graph shows the quantified Δ Lifetime. Data are quoted as the median (range), n=20 cells per condition. Pseudocolor scale: pixel-
850 by-pixel Δ Lifetime. Scale bar: 10 μ m.

I. p21^{Cip1} (top) and caspase 3 (bottom) immunoprecipitation in PBs. Caspase 3 and p21^{Cip1} were detected by immunoblotting.

J. p21^{Cip1}, procaspase 3, cleaved caspase 3 and cleaved PARP protein expression on D6 in PBs, after transfection with siCDKN1A or siCTL on D4.

855 **K.** On D4, activated B cells were treated for 24 h with increased doses of p21i in the presence or absence of Q-DEVD-OPH. PB viability (the proportion of active-caspase-3-negative cells) was assessed by flow cytometry. Data are quoted as the mean \pm SD, n=5.

L. The PIM2/p21^{Cip1}/caspase 3 pathway in PBs. p21^{Cip1} is stabilized in the cytoplasm
860 by a protein complex that also includes PIM2 and HSP90 β . Due to this localization, p21^{Cip1} interacts with procaspase 3 and blocks its activation.

A, H, K, Statistical significance was evaluated using Mann-Whitney (**A, H**) and Kruskal-Wallis (**K**) tests. * $P < 0.05$, ** $P < 0.01$, *** $P < 0.001$, **** $P < 0.0001$.

See also Fig. S5.

Fig 6. PIM2 in bone marrow plasma cells

A. *PIM2* mRNA expression in different tonsil-derived B cell populations (n=7) and in BM PCs (n=9). The data are quoted as the median (range).

B. Immunofluorescence staining of PIM2 (green) and CD138 (orange) on paraffin-
870 embedded normal BM. DAPI (blue) stains the nucleus. Scale bar: 20 μ m.

C. *PIM2* mRNA and PIM2 protein expression in CD23⁺ aBCs and PBs on D6 and ePCs on D10. Data are quoted as the median (range), n=10.

D. On D10, ePCs were sorted, starved and treated (or not) with an anti-R-IL6 mAb 1 h before stimulation. IL-6 and supernatants of BM mesenchymal stroma cells (s-MSc) were pre-incubated (or not) for 1 h with an anti-IL6 mAb. *PIM2* mRNA expression (left) and protein expression (right) in ePCs 5 h after the addition of IL-6 or s-MSc. Data are quoted as the mean \pm SD, n=4.
875

E. Immunofluorescence staining of PIM2 (green), CD41 (red) and CD138 (orange) on paraffin-embedded normal BM. DAPI (blue) stains the nucleus. Scale bar: 20 μ m.

F. On D9, cells were treated with PIMi. The proportion of active-caspase-3-positive cells was assessed on D10, using flow cytometry. Data are quoted as the mean \pm SD, n=6.
880

G. On D10, live cells were treated for 2 h with PIMi. Protein expression levels of caspase 9, XIAP, caspase 3, and p21^{Cip1} were assessed by immunoblotting.

H. p21^{Cip1} expression was assessed on D10 in nuclear & cytoplasmic fractions by immunoblotting and immunofluorescence. Sytox (blue) stains the nucleus. Scale bar: 5 μ m.
885

I. FRET/FLIM data were analyzed for ePCs stained for (the donor) PIM2 (left) or caspase 3 (right) in the presence or absence of p21^{Cip1} (the acceptor). The graph shows the quantified Δ lifetime. Data are quoted as the median (range), n=20 cells per
890

condition. Pseudocolor scale: pixel-by-pixel Δ lifetime. Scale bar: 10 μ m.

A, C, D, F, I, Statistical significance was evaluated using Mann-Whitney test. $*P < 0.05$, $**P < 0.01$, $***P < 0.001$, $****P < 0.0001$.

See also Fig S6.

895

Fig 7. Reconsideration of PIM2 as an effective target in multiple myeloma

A. *PIM2* gene expression in cell lines derived from various solid and blood cancers (<https://depmap.org/portal/>).

B. CRISPR screening data from the DepMap project show that *PIM2* presents the
900 highest dependency score for the 20 tested MM cell lines, relative to other cell lines.

C. Immunohistofluorescence staining of *PIM2* (green) and CD138 (orange) in paraffin-embedded BM from MM patients. DAPI (blue) stains the nucleus. Scale bar: 20 μ m (Top). Scale bar: 50 μ m (Bottom).

D. Overall survival of patients from the CoMMpass cohort as a function of *PIM2*
905 expression (PIM-high group; n=539 and PIM-low group (n=227)). The expression cutoff was determined by applying the MaxStat package (cutoff = 313.02).

E. Effects of BH3-mimetics and PIMi on apoptosis. BH3-mimetics (such as MCL1i and venetoclax) inhibit the binding of anti-apoptotic molecules (MCL1 and BCL2, respectively) to the pro-apoptotic effectors BAK and BAX; this leads to mitochondrial
910 depolarization and, ultimately, cell apoptosis. PIMi enhances BAD's action: BAD binds to BCL2 and BCL-XL and therefore acts independently of MCL1i. The combination of these two compounds might result in greater activation of BAX and BAK and might increase the likelihood of cell death.

F-G. Left, The results of a cell viability assay and a synergy analysis after treatment
915 with increasing concentrations of AZD1208 (PIMi) and AZD5991 (MCL1i) in XG7 cells

(**F**) and U266 cells (**G**). **Right**, Flow cytometry assessment of apoptosis using DAPI/CaspGlow staining and immunoblotting for the detection of caspase 3 and PARP cleavage, after treatment of XG7 cells (**F**) and U266 cells (**G**) with selected doses of inhibitors. The bar plot shows the percentage of caspase-3-active positive
920 cells. Data are quoted as the mean \pm SD, n=5.

H. Flow cytometry assessment of viability for primary cells from six MM patients. The bar plot shows the percentage of viable CD138⁺ MM cells and CD138⁻ cells, relative to a control (set to 100%) after treatment with the selected doses of inhibitor.

F, G, H, Statistical significance was evaluated using Mann-Whitney test. ****P** < 0.01.

925 See also Fig. S7.

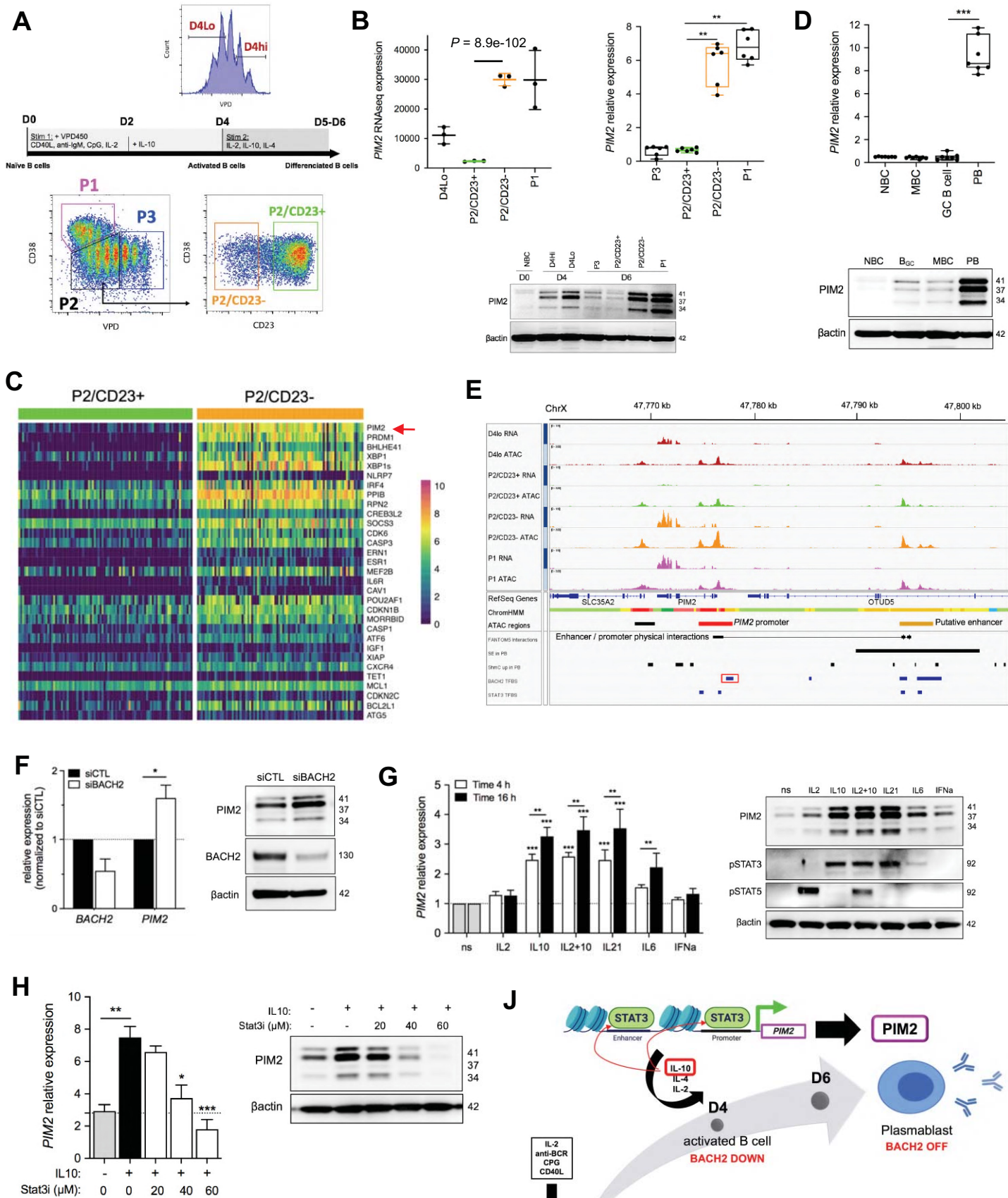


Fig. 1

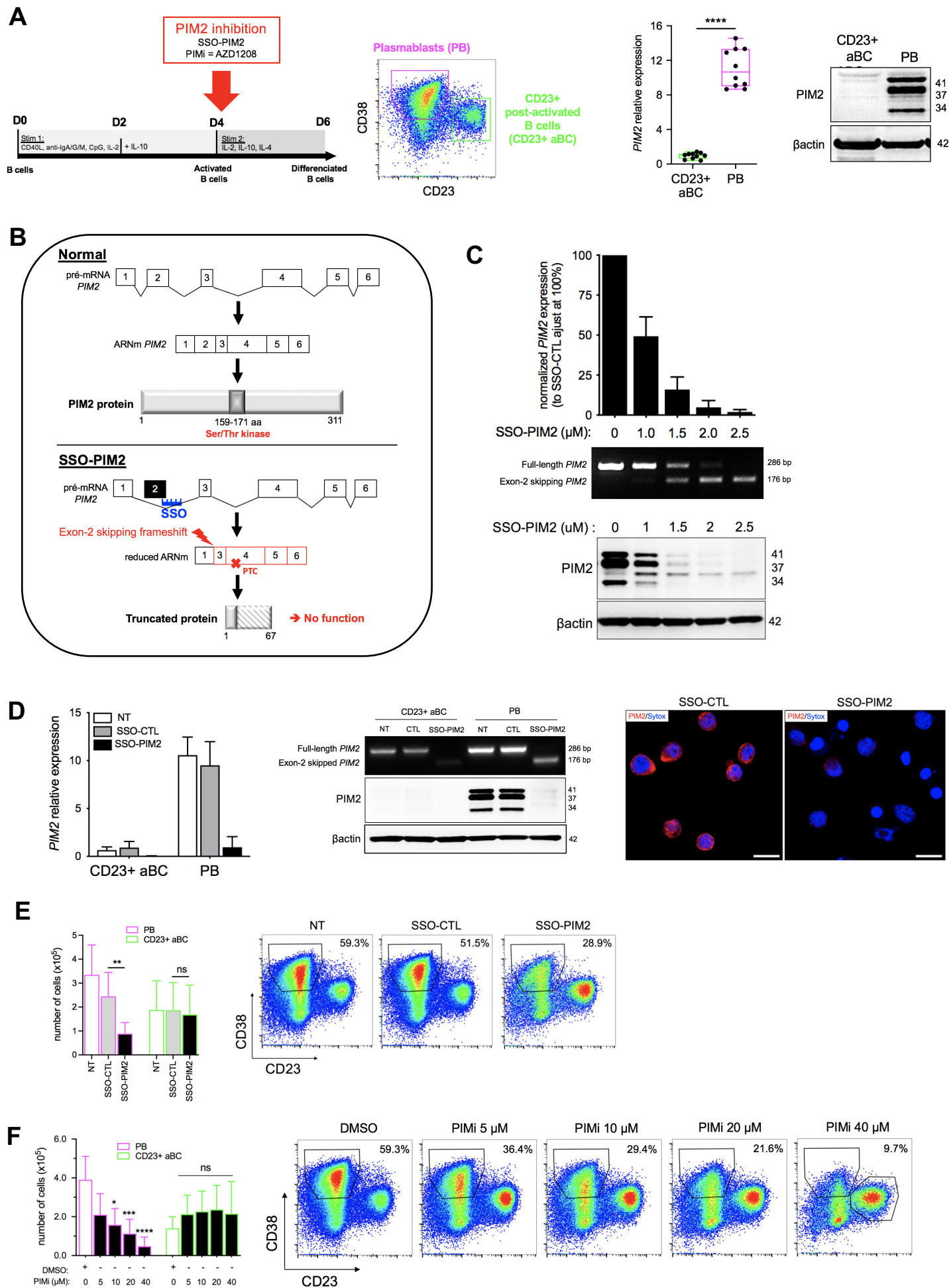


Fig. 2

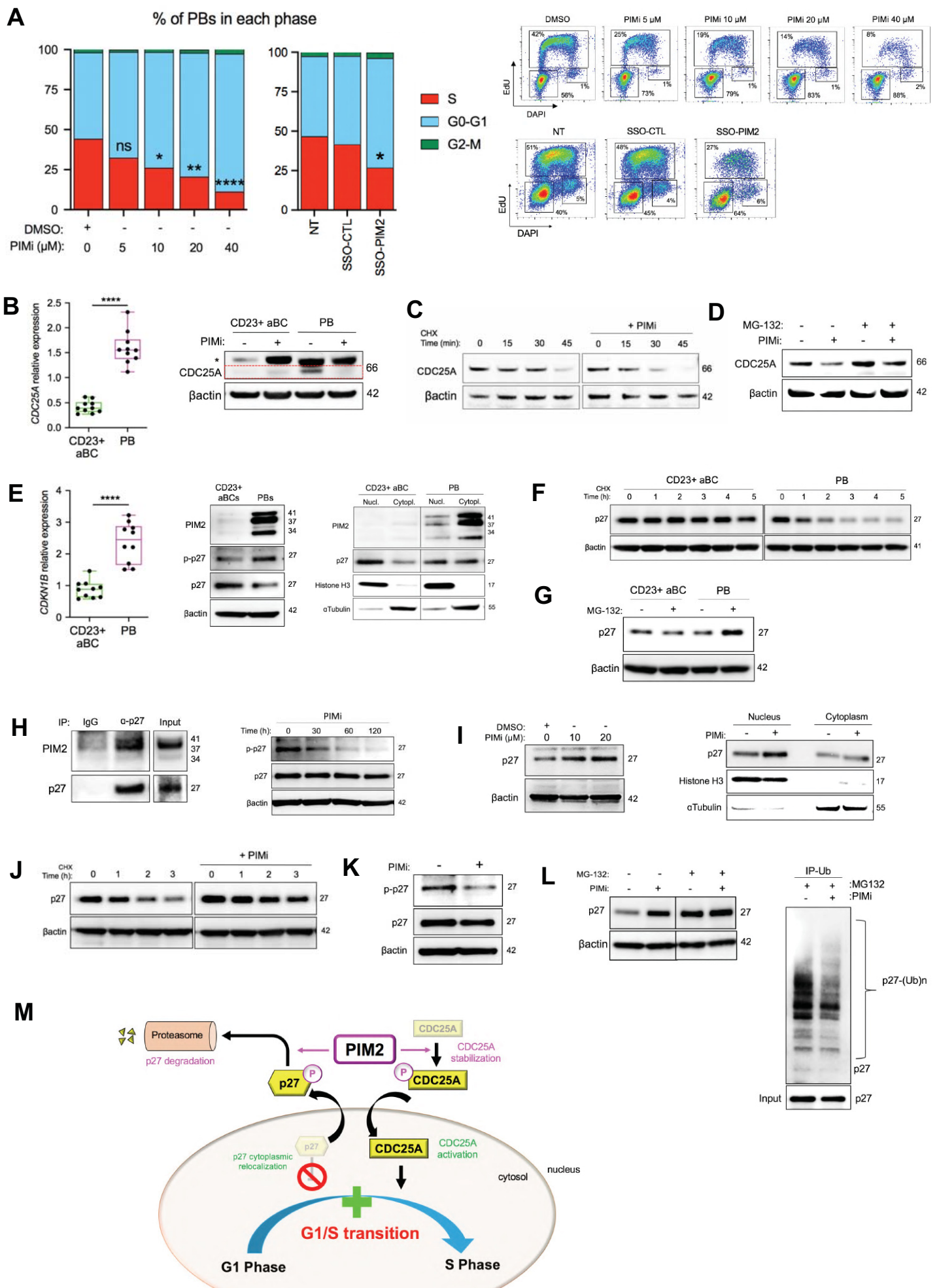


Fig. 3

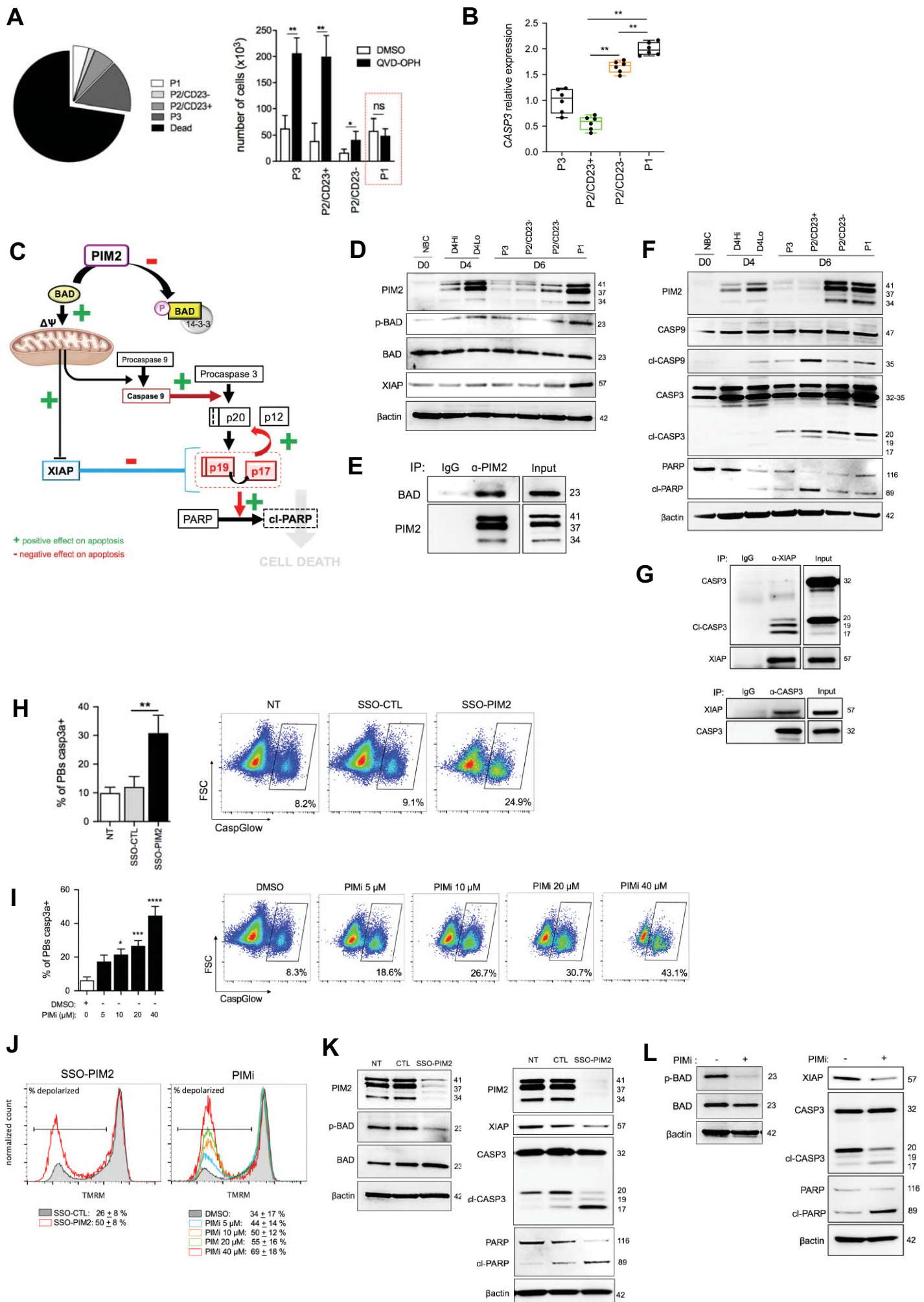


Fig. 4

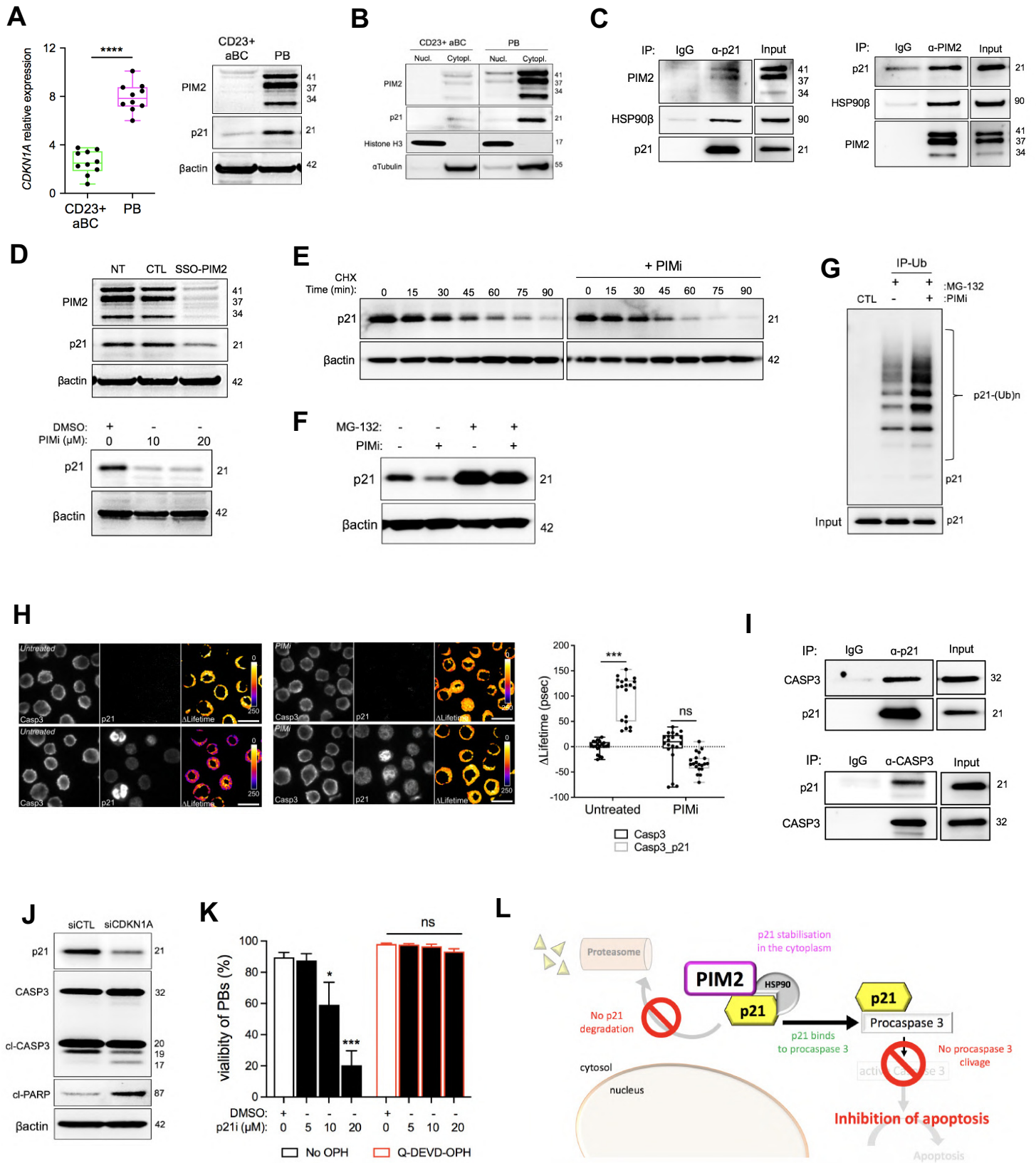


Fig. 5

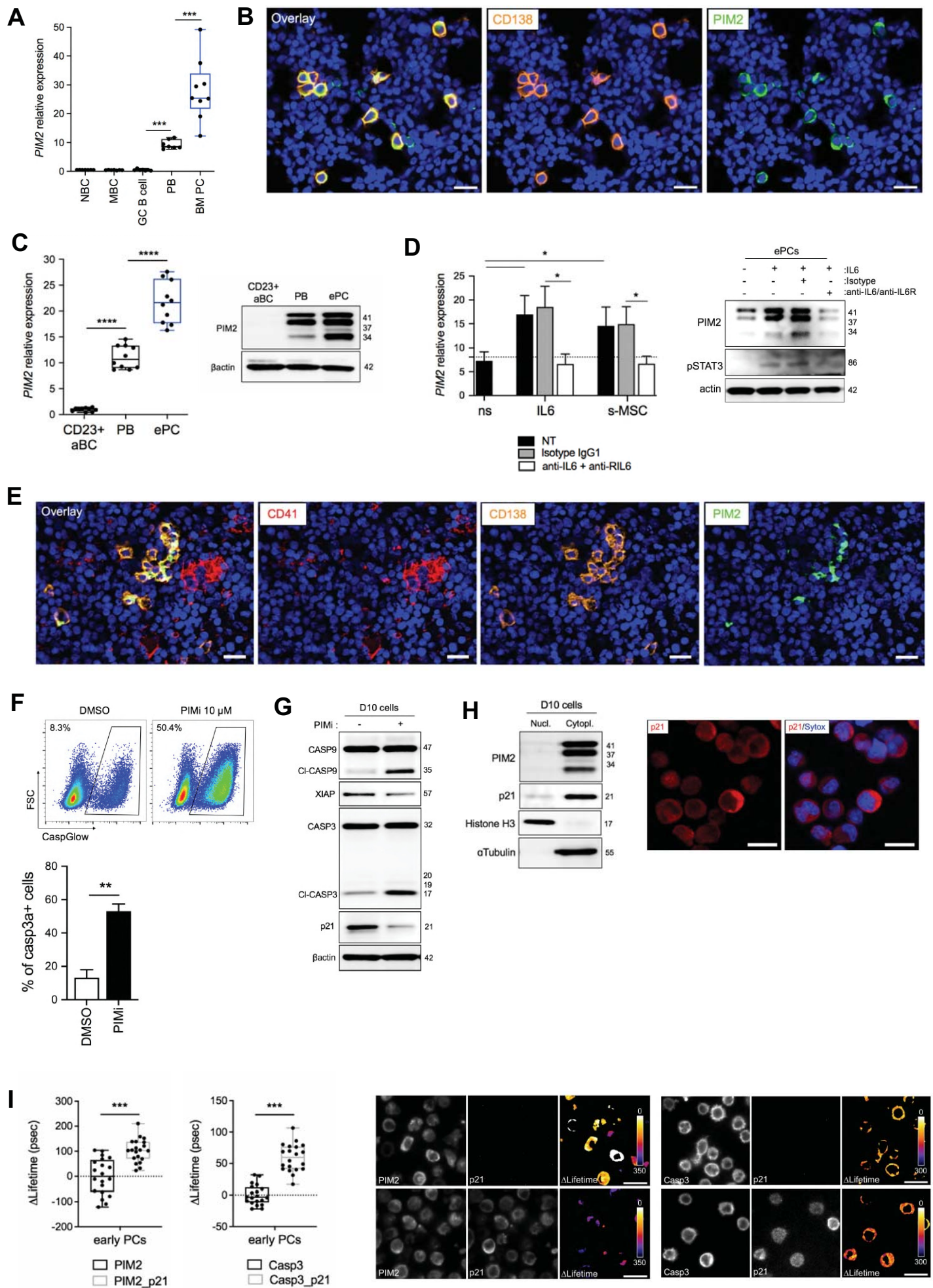


Fig. 6

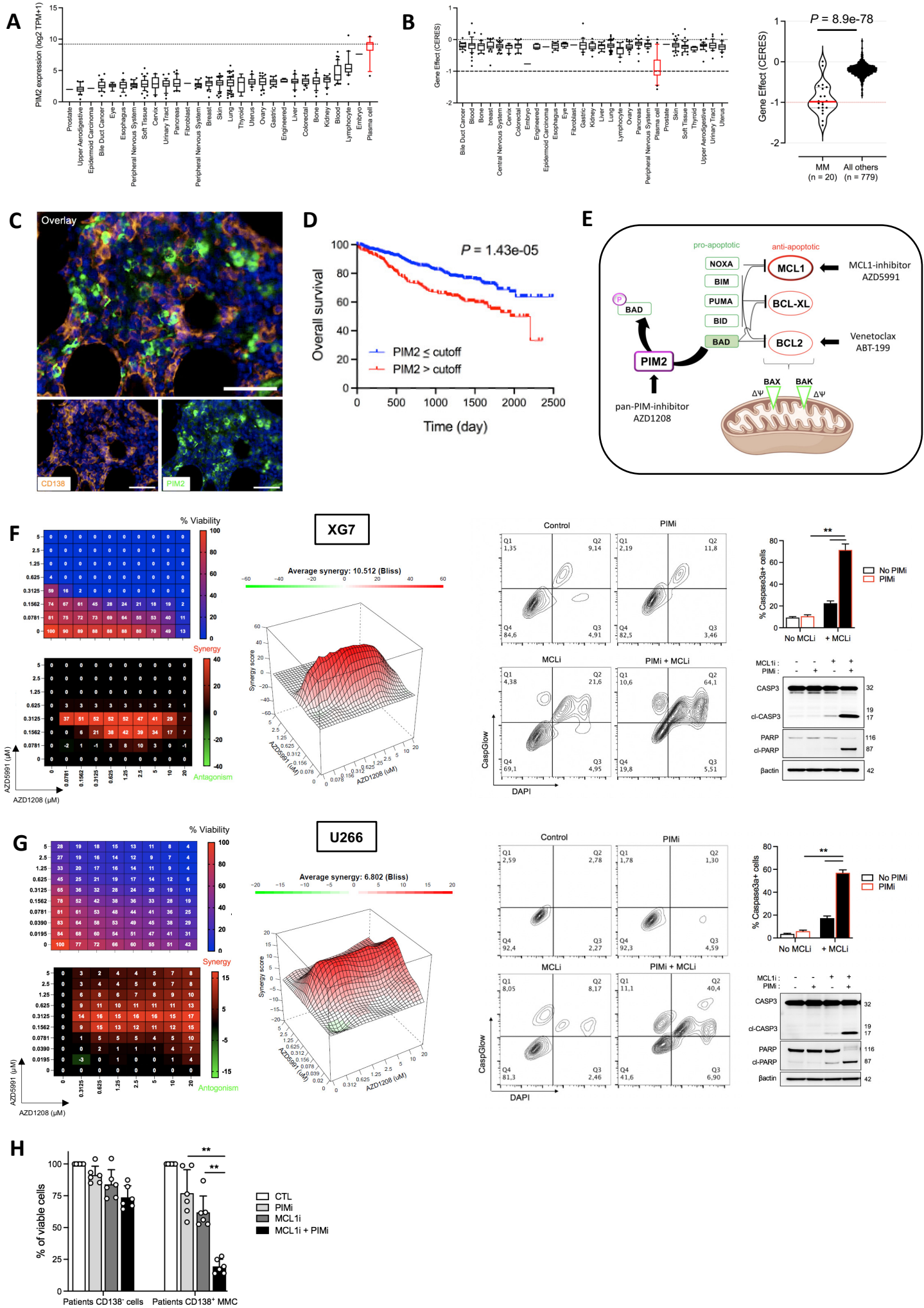


Fig. 7